A Comprehensive Mathematical Model for Three-Body Binding Equilibria

Eugene F. Douglass, Jr.,[†] Chad J. Miller,[‡] Gerson Sparer,[§] Harold Shapiro,[||] and David A. Spiegel*[,†,‡]

[†]Department of Chemistry and [‡]Department of Pharmacology, Yale University, New Haven, Connecticut 06520, United States
[§]Department of Mathematics, Pratt Institute, Brooklyn, New York 11205, United States
[||]Courant Institute of Mathematical Sciences, New York University, New York, New York 10012, United States

Ⓢ Supporting Information

ABSTRACT: Three-component systems are often more complex than their two-component counterparts. Although the reversible association of three components in solution is critical for a vast array of chemical and biological processes, no general physical picture of such systems has emerged. Here we have developed a general, comprehensive framework for understanding ternary complex equilibria, which relates directly to familiar concepts such as EC_{50} and IC_{50} from simpler (binary complex) equilibria. Importantly, application of our model to data from the published literature has enabled us to achieve new insights into complex systems ranging from coagulation to therapeutic dosing regimens for monoclonal antibodies. We also provide an Excel spreadsheet to assist readers in both conceptualizing and applying our models. Overall, our analysis has the potential to render complex three-component systems—which have previously been characterized as "analytically intractable"—readily comprehensible to theoreticians and experimentalists alike.
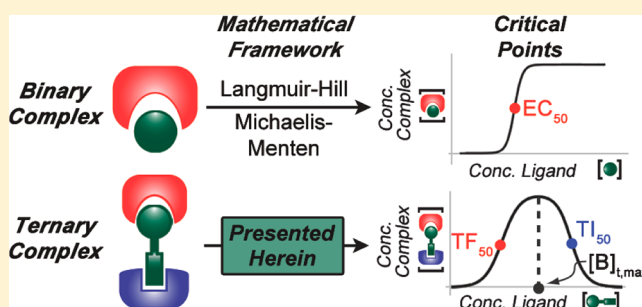
INTRODUCTION

Since Langmuir's initial mathematical characterization of binary complex equilibria in the early 20th century,[1] researchers have endeavored to describe the behavior of multicomponent complexes mathematically. Three-body (ternary complex) equilibria (Figure 1A) are ubiquitous in nature and critical for diverse systems-level processes including coagulation, antibody-mediated phagocytosis, and supramolecular assembly.[2–5] Despite extensive efforts, development of a complete framework for understanding ternary equilibria has proven elusive.[6] Of particular difficulty is that some ternary and higher-order equilibria exhibit a bell-shaped dose–response curve (Figure 1B), in which increasing the total concentration of the central species (here termed "B") can actually cause a *decrease* in ternary complex concentration ([ABC], Figure 1B).[7,8] Thus, there exists a total concentration of B ($[B]_{t,max}$) at which a maximal ternary complex concentration ($[ABC]_{max}$) is observed. This characteristic "bell-shaped" binding curve was first observed in 1905 in immunoprecipitation assays and coined the "prozone phenomenon".[9] Over the past century, prozone behavior has been observed in a large number of systems, and has been given several field-specific names including the "hook effect",[10] "auto-inhibition",[11] "template mechanism",[12] "combinatorial inhibition",[6] and "dose-limited activity".[13]

A "holy grail" in characterizing ternary binding interactions mathematically has been to identify analytical expressions that can relate [ABC] to measurable parameters—total concentrations ($[A]_t$, $[B]_t$, and $[C]_t$) and equilibrium dissociation constants (K_{AB} and K_{BC}).[14,15] Such mathematical models must also account for interactions between "A" and "C" in the ternary complex, termed "cooperativity", and represented by the symbol α (Figure 1C,D).[16] A system is termed positively cooperative ($\alpha > 1$) or negatively cooperative ($\alpha < 1$) when interactions between A and C enhance or diminish formation of ABC complex, respectively (Figure 1D).[16–18] To model this system, many researchers have invoked either various simplifying assumptions[4,19–23] or complex numerical simulations.[6,24,25] Exact analytical models, on the other hand, are the only mathematical models which provide physical insight over a comprehensive set of conditions; thus, conceptual frameworks can only be considered "complete" when based on such models.[16,26,27]

Recent theoretical analyses of the multicomponent equilibria involved in supramolecular assembly has enabled physical understanding of related bell-shaped curves. Unfortunately, no analogous treatment of ternary complex equilibria has emerged in spite of its relative simplicity (e.g., lacking additional complications such as statistical factors, chelate cooperativity, and polymerization).[28–30]

Here we rigorously derive a set of exact mathematical models that describe ternary complex equilibria by relating concentrations of solution species to measurable parameters (total

concentrations and dissociation constants). We conceptualize these models by adapting familiar concepts from binary complex equilibria. To this end, we define ternary complex curve "critical points", which include the height ($[ABC]_{max}$), position of the maximum ($[B]_{t,max}$), and the position of the half-maximal responses on the left (termed "<u>T</u>ernary <u>F</u>ormation 50%", or TF_{50}) and right (termed "<u>T</u>ernary <u>I</u>nhibition 50%", or TI_{50}) sides of the curve (Figure 1B). Application of our model to data from the published literature has enabled us to achieve new insights into complex systems that range from coagulation proteins to therapeutic dosing regimens for monoclonal antibodies. To help readers utilize our models, we also provide a detailed Excel spreadsheet (see Supporting Information (SI)) that contains several salient features of our models. Overall, the comprehensive analytical framework provided herein will enable both theoreticans and experimentalists to understand the complexities of ternary equilibria.
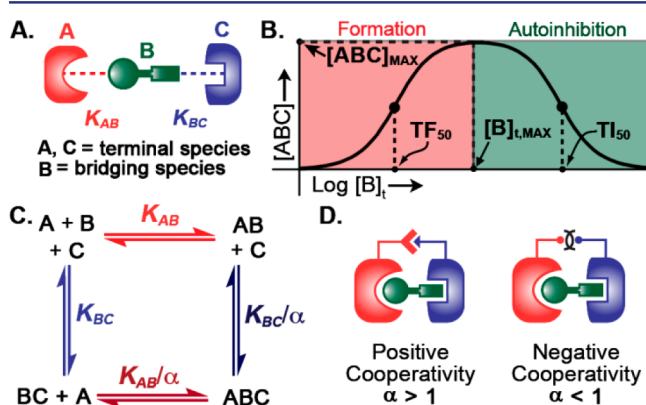

Figure 1. (A) Structure of ternary complex and definition of terminology for interacting components. (B) Graph depicting ternary complex concentration ($[ABC]$) as a function of total bridging species ($[B]_t$) and illustrating auto-inhibition. This curve can be understood in terms of critical points: the maximum concentration of ternary complex that can be achieved ($[ABC]_{max}$), the concentration of $[B]_t$ required to achieve $[ABC]_{max}$ ($[B]_{t,max}$), and the $[B]_t$ values that elicit half-maximal $[ABC]$ formation on the left (TF_{50}) and right (TI_{50}) sides of the curve. (C) Thermodynamic cycle for the reversible formation of ternary complexes. (D) Illustrations and mathematical definitions for positive and negative cooperativity.

RESULTS AND DISCUSSION

Non-cooperative Equilibria. We have explicitly proven that expressions for solution species ($[ABC]$, $[AB]$, $[C]$, etc.) in terms of cooperativity (α) and standard parameters (K_d's and total concentrations) cannot be obtained algebraically (SI, Section 2). Non-cooperative systems, in which terminal species A and C are incapable of interacting within ternary complexes ($\alpha = 1$), have proven simpler.[31] The equation for $[ABC]$ adopts a form where ternary complex concentration is expressed as a function of the product of two quadratic roots—termed ϕ_{AB} and ϕ_{BC}.[31]

Equation 1 can be rewritten in a normalized form as eq 2, wherein the left and right terms pertain exclusively to A−B and B−C binding interactions, respectively. Further inspection reveals that ϕ_{AB} and ϕ_{BC} are each formally identical to the general expression that governs binary binding interactions (Figure S1). Such binary complex curves are extremely well characterized and can be described—assuming the two

$$[ABC] = \frac{\phi_{AB}\phi_{BC}}{[B]_t} =$$

$$\frac{\left(\dfrac{[A]_t + [B]_t + K_{AB} - \sqrt{([A]_t + [B]_t + K_{AB})^2 - 4[A]_t[B]_t}}{2}\right) \times \left(\dfrac{[C]_t + [B]_t + K_{BC} - \sqrt{([C]_t + [B]_t + K_{BC})^2 - 4[C]_t[B]_t}}{2}\right)}{[B]_t} \quad (1)$$

$$\frac{[ABC]}{[A]_t} = \frac{\phi_{AB}}{[A]_t}\frac{\phi_{BC}}{[B]_t} \quad (2)$$

components are R (receptor) and S (substrate)—in terms of two critical parameters: the EC_{50} (<u>E</u>ffective <u>C</u>oncentration <u>50</u>%, which is equal to $K_{RS} + [R]_t/2$) and the saturating height, $[RS]_{max}$ (which is equal to the total concentration of the limiting species R, here abbreviated $[R]_t$).[32]

A useful situation arises when the A−B ($[A]_t + K_{AB}$) and B−C ($[C]_t + K_{BC}$) binding parameters differ by at least 1 order of magnitude. Under such conditions, the left and right sides of the ternary binding curve graphically "resolve" into functions of A−B and B−C binding events, respectively. In other words, when $[B]_t < [B]_{t,max}$, $[ABC]$ (Figure 2A, black curve) exclusively reflects the behavior of ϕ_{AB} (red curve), while for $[B]_t > [B]_{t,max}$, $[ABC]$ reflects the behavior of ϕ_{BC} (blue curve).[33] At $[B]_{t,max}$ (pink vertical line), both formation and auto-inhibition curves equal their plateau y-axis values, such that

$$\frac{[ABC]^R_{max}}{[A]_t} = \frac{[C]_t}{K_{BC} + [C]_t} \quad (3)$$

where the R superscript refers to resolvable conditions.

Half-maximal (TF_{50} and TI_{50}) values for resolvable systems can be written as

$$TF^R_{50} = K_{AB} + \frac{[A]_t}{2} \quad (4)$$

and

$$TI^R_{50} = \frac{2(K_{BC} + [C]_t)^2}{2K_{BC} + [C]_t} \quad (5)$$

Complete derivations of these expressions as well as a treatment of error associated with the resolvability assumption are provided in the SI, Section 5.

Further simplification of non-cooperative critical parameter expressions can be achieved through the "dominance" assumption. In systems with a dominant parameter, the K_d and total concentration of a specific binary interaction differ by a factor of 10 or greater (Figure S1). Binary complex equilibria have classically been understood with respect to dominance of either the K_{RS} or $[R]_t$ parameter (see ref 34 and SI, Section 1). When the dissociation constant governing a binary interaction is much greater than the total limiting reagent concentration ($K_{RS} \gg [R]_t$)—termed "Langmuir−Hill" conditions—the EC_{50} reduces to the K_{RS}. When $[R]_t \gg K_{RS}$, on the other hand, the system exhibits "saturating binding behavior", and the position of the inflection point of the curve (EC_{100}, or $[R]_{t,max}$) is equal to $[R]_t$.[34] A similar analysis can be made for each of the binary binding events in eq 1; the dominance assumption, therefore,
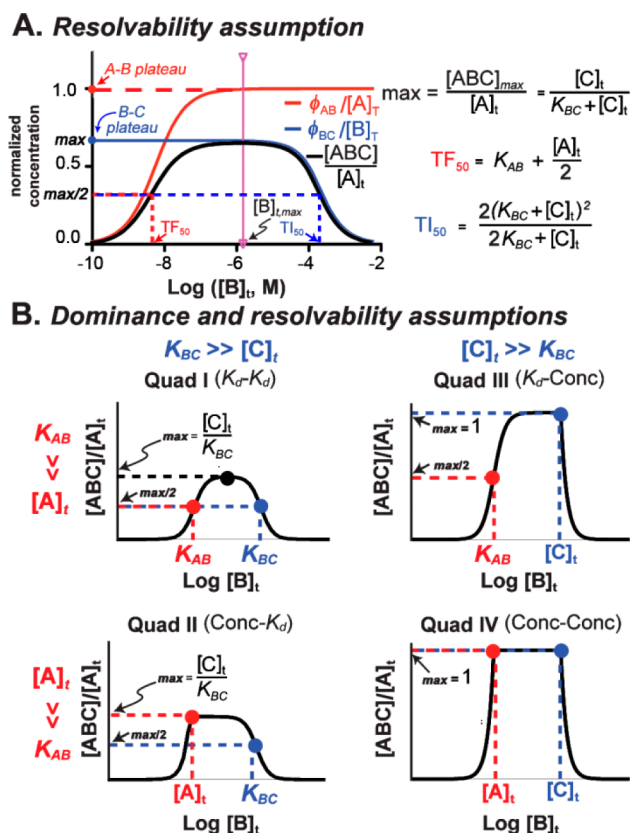
Figure 2. (A) A non-cooperative, bell-shaped ternary complex dose−response curve (black curve) can be explained by a sigmoidal "formation" term (red curve) and a reversed sigmoidal "auto-inhibition" term (blue curve). When both of these curves are plateaued at $[B]_{t,max}$, the left side of the ternary complex curve (black curve) is described by the A−B binding event (TF_{50}), whereas the right side is described by the B−C binding event (TI_{50}). (B) Non-cooperative systems can be divided into four quadrants, which enable simplification of $[ABC]_{max}$, $[B]_{t,max}$, TF_{50}, and TI_{50} equations. Regarding the height (y-axis, or $[ABC]_{max}$), ternary complex does not form appreciably in Quadrants I and II but forms quantitatively in Quadrants III and IV. The width and position (x-axis, or TF_{50}, TI_{50}, and $[B]_{t,max}$) of these curves are controlled by either the binding constants (Quadrant I), the terminal species concentrations (Quadrant IV), or a combination of both (Quadrants II and III). Red indicates A−B binding event; blue indicates B−C binding event.

enables us to group non-cooperative ternary complexes into four limiting scenarios, which we term "Quadrants", depending on which parameter is greater (either K_d or concentration) for A−B and B−C components of binding curves (Figure 2B). This picture, although simple, is nevertheless applicable under the majority of experimental conditions we have encountered in the published literature.

In Quadrant I, for example, $K_{AB} \gg [A]_t$ and $K_{BC} \gg [C]_t$. Considered in light of eqs 4 and 5, the TF_{50} and TI_{50} values reduce to K_{AB} and K_{BC}, and $[B]_{t,max}$ (eq S34) can be simplified to $(K_{AB} \times K_{BC})^{1/2}$. Also, the normalized height ($[ABC]_{max}/[A]_t$, eq 3) reduces to $[C]_t/K_{BC}$, which cannot attain a value greater than 0.1 because $K_{BC} \gg [C]_t$ in this quadrant. Experimental systems whose physical behaviors are well-described by Quadrant I often involve terminal species confined to small regions of space (such as cell surfaces) such as antibody-induced basophil degranulation, receptor-mediated phagocytosis, and antibody-dependent cellular cytotoxicity.[3,13,21]

Quadrant IV can be considered the opposite of Quadrant I (Figure 2D). Here $K_{AB} \ll [A]_t$ and $K_{BC} \ll [C]_t$ such that both left and right sides of ternary binding curves exhibit saturation binding behavior. Binding equilibria in this quadrant therefore possess flat plateaus extending from $[A]_t \leq [B]_t \leq [C]_t$, with sharp transitions between the plateau and formation/auto-inhibition sides of the curve.[35] Systems that can be categorized into Quadrant IV often involve terminal species that are highly expressed, such as scaffold protein complexes.[6,36]

Equilibria classified in Quadrants II and III can be understood as hybrids between Quadrants I and IV, and they exhibit mixed Langmuir−Hill and saturation binding behaviors. The Quadrant II regime, for example, is characterized by extremely low ternary complex concentrations because the right side of the curve—which defines $[ABC]_{max}$ (eq 3)—can never be greater than $[C]_t/K_{BC}$. Quadrant III, on the other hand, exhibits near quantitative ternary complex formation. Derivations of the critical points for these systems, along with detailed treatments of error, are presented in the SI, Section 5.

Non-cooperative Experimental Systems. Examination of the published literature has revealed that the simple non-cooperative framework presented in the preceding section can provide insights into several important experimental systems. One such example is antibody-dependent cell-mediated cytotoxicity (ADCC). This process is essential for humoral immune responses, and also for the efficacy of the therapeutic monoclonal antibodies Herceptin and Rituxan,[37] which have emerged as important anticancer agents. Antibodies elicit ADCC by forming ternary complexes between Fc-gamma receptors (FcγRs) on immune cells and disease-specific markers on cancer cells. Indeed, bell-shaped dose−response curves have been observed for antibody-mediated activities (e.g., cytotoxicity and phagocytosis) both *in vitro* and *in vivo*.[13,38,39] In one published example, treatment of A498 renal carcinoma cells—which overexpress the receptor tyrosine kinase ephrin A2 (EphA2)—with an anti-EphA2 antibody (3F2) at various concentrations led to observation of an auto-inhibitory cell lysis curve (Figure 3A) following exposure to immune cells from peripheral blood.[13]

Because both terminal species—the cancer marker EphA2 and Fc receptors on immune cells—are restricted to cell surfaces, we expect ADCC in this assay to occur under conditions described by Quadrant I. Indeed, as predicted for this quadrant, TF_{50} and TI_{50} values closely resemble the K_d values measured for the EphA2−3F2 and IgG−Fc receptor interactions.[37] Furthermore, the concentration of antibody at which our model predicts maximal cytotoxicity ($(K_{AB}K_{BC})^{1/2}$ = 6 nM, see SI, Section 5C) is nearly identical to that determined experimentally (6.7 nM). Our model also provides guidelines for how ADCC will vary with changes in the experimental system. Because the antibody−Fc receptor interaction is weaker than the antibody−EphA2 interaction (and is therefore categorized as B−C in this example), improvements in ADCC efficacy would be expected to occur only upon optimizing the strength of this interaction (i.e., K_{BC}, see eq 3).[37] Although some authors have reached a similar conclusion empirically,[37] many have endeavored to improve antibody drug efficacy by increasing antibody−antigen affinities rather than antibody affinities for Fc receptors.[40−42] Our results provide a useful set of guidelines, along with a cohesive rationale, for how to optimize the cytotoxic function of antibodies. Notably, these results are readily extended beyond this specific mAb and can be used to accurately predict the clinical dose and $[B]_{t,max}$ of
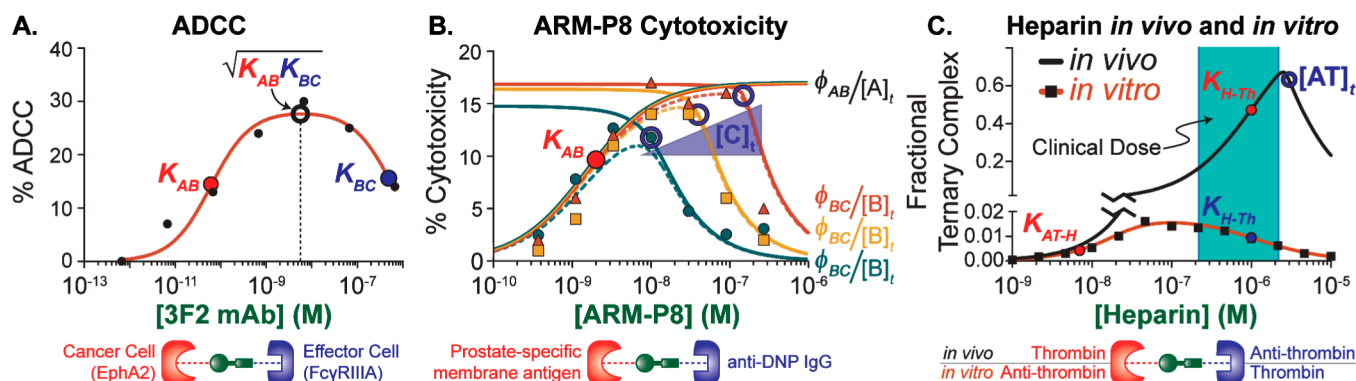
Figure 3. Non-cooperative ternary complexes in the literature. For each example, elements of the relevant ternary complex are defined by the keys located below each graph. (A) The dose−response curves of mAbs-mediating immune responses can be best explained via Quadrant I (Figure 2B) as observed in the anti-renal carcinoma mAb 3F2 (data from ref 13; binding constants from ref 37). (B) Antibody-Recruiting Molecules targeting Prostate cancer (ARM-Ps) also exhibit bell-shaped dose−response curves characterized by Quadrant III (Figure 2B).[43] Even as the resolvability assumption breaks down, Quadrant III closely approximates the system's behavior. Dashed lines represent the predicted ternary complex curves, and solid lines represent the two ϕ terms; ϕ_{AB} is a constant, whereas ϕ_{BC} changes with increasing $[C]_t$, which is 10 nM (green curve), 40 nM (yellow curve), and 160 nM (red curve). (C) Differences between the *in vitro* and *in vivo* potency and efficacy of heparin can be explained by the fact the former is a Quadrant I system (predicted curve in red, data from ref 2), whereas the latter is a Quadrant III system (predicted curve in black, clinical dose estimates from ref 47). ADCC, antibody-dependent cell-mediated cytotoxicity; mAb, monoclonal antibody; DNP, dinitrophenyl.

other mAbs, such as Abegrin, where the *in vitro* $[B]_{t,\mathrm{max}}$ and the clinical dose are equal to $(K_{AB}K_{BC})^{1/2}$.[13]

Of course, because our analysis is based on exact models, we can obtain insights into experimental systems even when dominance and resolvability conditions are not met. Analysis of data from our laboratory's development efforts toward antibody-recruiting molecules targeting prostate cancer ("ARM-Ps") serves as evidence of this fact.[43] ARM-Ps mediate ternary complex formation between anti-dinitrophenyl (anti-DNP) IgG antibodies and the cancer marker prostate-specific membrane antigen (PSMA).[44] Cytotoxicity measurements exhibit prozone behaviors at increasing concentrations of ARM-P (Figure 3B), yet unlike in the previous example, this system is best described by Quadrant III.[45] At the highest $[C]_t$ values (yellow and red curves), the calculated plateaus of $\phi_{AB}/[A]_t$ and $\phi_{BC}/[B]_t$ overlap at $[B]_{t,\mathrm{max}}$ with each other and experimental observations conform almost exactly to the ideal behavior predicted for Quadrant III (yellow and red curves, dashed lines), enabling ready determination of critical points (i.e., $K_{AB} = \mathrm{TF}_{50}$ and $[C]_t = [B]_{t,\mathrm{max}}$). The resolvability assumption does not hold at the lowest value of $[C]_t$ (green curve), because K_{AB} is only 6-fold lower than the value of $[C]_t$. Therefore, the plateaus of $\phi_{AB}/[A]_t$ and $\phi_{BC}/[B]_t$ do not overlap at $[B]_{t,\mathrm{max}}$, and K_{AB} slightly overestimates the value of the TF_{50}. In addition, because $[C]_t$ is only 10 times greater than K_{BC} at this antibody concentration, the dominance assumption begins to break down, resulting in slight overestimation of the $[B]_{t,\mathrm{max}}$ (SI, Section 5D,E).

Several useful conclusions about how ARM-Ps might behave *in vivo* can be drawn from this analysis. Under conditions when the dominance condition holds, ternary complex concentration depends exclusively on two parameters—K_{AB} and $[C]_t$. Specifically, K_{AB} controls the value of the TF_{50}, or the apparent "potency" of ARM-Ps, whereas $[C]_t$ dictates the value of $[ABC]_{\mathrm{max}}$, or ARM-P "efficacy". Conversely, variations in non-dominant parameters ($[A]_t$ and K_{BC}) do not affect ternary complex levels. For example, decreases in the count of malignant cells occurring during the course of ARM-P treatment, which lead to changes in $[A]_t$, are unlikely to perturb therapeutic effectiveness. Similarly, although one might

intuitively expect that optimization of the antibody−ARM-P K_d (K_{BC}) would enhance ARM-P performance, alteration of this parameter is unlikely to have any measurable effect. Rather, the only strategy likely to improve the cytotoxic properties of ARM-Ps is to increase antibody levels ($[C]_t$). These and other predictions arising from our model have already proven useful in the ongoing preclinical development of these compounds.[46]

Understanding the critical factors for determining ternary complex concentration has enabled us to resolve an apparent discrepancy related to therapeutic control of blood coagulation. Heparin is a potent anti-coagulant that exerts its effects, in part, by bringing together the pro-coagulant serine protease thrombin with its inhibitor anti-thrombin (Figure 3C). It has been observed that the values of heparin that lead to maximal anti-coagulation *in vitro* (i.e., the $[B]_{t,\mathrm{max}}$) do not correlate with clinical dosing levels. In fact, heparin dosages found to elicit ideal anti-coagulant behavior in humans would be predicted to be sub-optimal, or even inactive, *in vitro* because they fall within the auto-inhibitory region of ternary complex curves (Figure 3C).[2,47] This discrepancy has led to some confusion in the published literature.[47,48]

Understanding the profound effect that a single parameter can have on ternary complex dynamics is the key to resolving this apparent inconsistency. *In vitro*, researchers employed relatively low concentrations of anti-thrombin (perhaps to render the system tractable to biochemical or enzymological study). Under these conditions, the anti-thrombin−heparin and heparin−thrombin complexes occupy A−B and B−C binding positions, respectively, and the system most closely fits a Quadrant I model. *In vivo*, on the other hand, the concentration of anti-thrombin is more than 2 orders of magnitude higher than it is *in vitro*.[47] This marked concentration increase *in vivo* causes the identities of A−B and B−C to reverse; thrombin−heparin becomes A−B and heparin−anti-thrombin becomes B−C. Furthermore, the anti-thrombin concentration ($[C]_t$ *in vivo*) is in great excess over the heparin−anti-thrombin dissociation constant (K_{BC}). Therefore, a Quadrant III model is most apt for this system *in vivo* (rather than Quadrant I as *in vitro*). The switch between these quadrants has two critical effects on ternary equilibria: first, the height of the curve (eq 3)
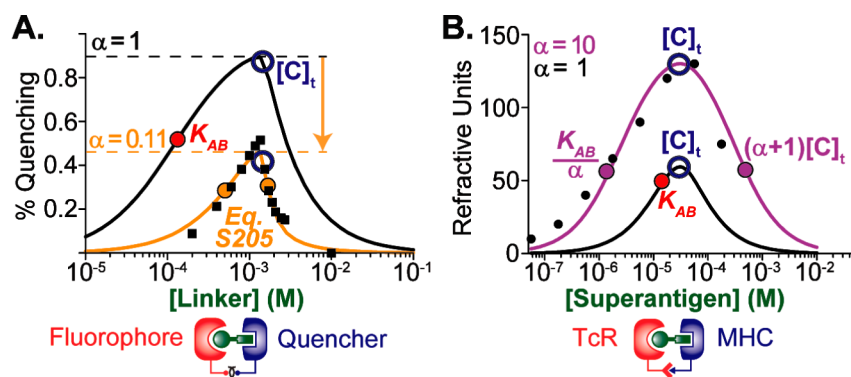
Figure 4. Cooperative perturbation of the quadrant framework. The black curves in each plot corresponds to a non-cooperative reference equivalent to what is presented in Figure 2B. The purple curves show the effect of cooperativity when $\alpha > \alpha_{crit}$ (width perturbation), and the orange curves show the effect of cooperativity when $\alpha < \alpha_{crit}$ (height perturbation). Cooperative TF_{50} and TI_{50} expressions are presented in boxes and represent the $[B]_t$ value for the point. Overall, Quadrants I and II do not form appreciable ternary complex when $\alpha = 1$, and the effect of positive cooperativity is to first increase the height and then increase the width; Quadrants III and IV form quantitative ternary complex when $\alpha = 1$, and positive cooperativity predominantly increases the width of these curves. $TPF = [ABC]_{max}/[L]_t$. The Quadrant II $\alpha > \alpha_{crit}$ TF_{50} shown above is correct when A is the limiting reagent; otherwise it equals eq S181.

should increase dramatically in Quadrant III (*in vivo*) compared to Quadrant I (*in vitro*, see Figure 3C), and second, $[B]_{t,max}$ (eq S34) should occur at a much higher heparin concentration in Quadrant III (*in vivo*) versus Quadrant I (*in vitro*, see Figure 3C). These trends explain both heparin's lower potency and higher efficacy *in vivo* versus what would be predicted on the basis of an intuitive extrapolation of *in vitro* data. Application of our analytical model to this system enables a straightforward rationale for heparin's clinical dosing patterns.

Cooperative Equilibria. Cooperative effects, which result from interactions between terminal species within ternary complexes, add an additional dimension of complexity to understanding ternary complex equilibria (Figure 4). Indeed, it has previously been stated that no analytical solution exists for [ABC] as a function of measurable parameters and the cooperativity term, α, and we have explicitly proven this assertion (see SI, Section 2). Recognizing that algebraic solvability is fundamentally directional (i.e., the fact that y is unsolvable in terms of x does not necessarily imply that x is unsolvable in terms of y), however, we sought an expression for $[B]_t$ as a function of [ABC] and measurable parameters. Indeed, algebraic rearrangement of eqs S1−S6 yields such an

analytical expression (eq 6). This "backwards" approach is possible when the entire range of y-axis values is known (i.e., from 0 to $[ABC]_{max}$) because eq 6 can be used to determine all x-axis values including $[B]_{t,max}$, TF_{50}, and TI_{50}.

$$[B]_t = \left(\begin{array}{c} [A]+[C]_t - K_{AB} - K_{BC} + \dfrac{\alpha\big([ABC]-[A]_t\big)\big([ABC]-[C]_t\big)}{[ABC]} \\[4mm] + \dfrac{[A]_t\big(K_{BC}-K_{AB}\big)}{\alpha\big([ABC]-[A]_t\big)} + \dfrac{[C]_t\big(K_{AB}-K_{BC}\big)}{\alpha\big([ABC]-[C]_t\big)} \pm \\[4mm] \dfrac{1}{2}\left(\dfrac{\alpha}{[ABC]}+\dfrac{1}{[A]_t-[ABC]}+\dfrac{1}{[C]_t-[ABC]}\right)\times \\[4mm] \dfrac{\sqrt{\begin{array}{l}\big(\alpha\big([ABC]-[A]_t\big)\big([ABC]-[C]_t\big)-[ABC]K_{AB}\big)^2 - \\ 2[ABC]K_{BC}\big(\alpha\big([ABC]-[A]_t\big)\big([ABC]-[C]_t\big)+[ABC]K_{AB}\big)+ \\ {[ABC]}^2 K_{BC}^2\end{array}}}{\alpha} \end{array}\right) \tag{6}$$

Using eq 6 as a guide, we have developed a comprehensive model to explain the effects of cooperativity as perturbations of

Figure 5. Examples of Quadrant III cooperative ternary complexes. (A) Supermolecular assembly: the effects of negative cooperativity can be understood as a reduction in the height (eq 7) and width (eq S205) of a Quadrant III non-cooperative curve (data from ref 4). (B) Antigen presentation: the effects of positive cooperativity can be understood as an increase in the height (eq 7) and/or width (eqs S191 and S192) of a Quadrant III non-cooperative curve (data from ref 20). The TF_{50} and TI_{50} expressions simplify for each quadrant, enabling conceptualization of the width as a perturbation on the non-cooperative reference curve.

non-cooperative equilibria. As shown graphically in Figure 4, both the height and width of cooperative binding curves deviate substantially, yet predictably, from the non-cooperative reference curve (black curves) as a function of α. In general, cooperativity-induced perturbations can manifest as alterations in the height (i.e., $[ABC]_{max}$) and/or the width (i.e., the distance between TF_{50} and TI_{50} values) of non-cooperative ternary complex curves. The tendency to experience either a height or a width perturbation can be predicted based on the value of $[ABC]_{max}/[L]_t$ ($[L]_t$ corresponds to the concentration of the limiting terminal species) for a particular non-cooperative system. We define the quantity $[ABC]_{max}/[L]_t$ as the "ternary partition fraction" (abbreviated "TPF") because it represents the maximal amount of the limiting terminal species that can partition into ternary complex for a given set of parameters. Cooperative perturbations predominantly affect curve width when the TPF exceeds 0.5 (Figure 4, purple curves), and they predominantly affect curve height once TPF values decrease below 0.5 (Figure 4, orange curves). This can be observed graphically in Figure 4: systems that possess non-cooperative TPF values less than 0.5 (i.e., black curves in Quadrants I or II) will experience height alterations with modest changes in α, whereas those with non-cooperative TPF values greater than 0.5 (i.e., black curves in Quadrants III or IV) will vary in width. Large changes in α, however, can result in both height and width perturbations relative to the non-cooperative curve. For example, a Quadrant I system with large positive cooperativity could experience both a height increase and width expansion.

Because the TPF is so useful in predicting the type of perturbation a system will undergo in response to cooperativity, it is useful to define this concept mathematically. $[ABC]_{max}$ can be expressed analytically as shown in eq S37, which is similar in form to a generic binary complex binding equation. Application of the Langmuir assumption and dividing by $[L]_t$ simplifies eq S37 to

$$\frac{[ABC]_{max}}{[L]_t} = \frac{\alpha}{\alpha + K_{weak}/[X]_t} \qquad (7)$$

without introduction of pronounced error (SI, Section 6E), such that the TPF depends exclusively on $[X]_t$ (the excess terminal species), K_{weak} (the weaker [i.e., larger] binding constant), and α (SI, Section 6C). In further analogy to the

Langmuir equation, one can define a value of α at which the TPF will equal 0.5, written as

$$\alpha_{crit} = \frac{K_{weak}}{[X]_t} \qquad (8)$$

For all systems, α_{crit} corresponds to the cooperativity value at which 50% of the limiting reagent will be engaged in ternary complex, as well as the transition point between predominant width and height perturbations (Figure 4, $\alpha = \alpha_{crit}$ at dashed gray lines). Because the dominant B–C parameter (either K_{BC} or $[C]_t$) is, by definition, always either K_{weak} or $[X]_t$, the value of eq 7 will always be below unity for non-cooperative systems in Quadrants I and II and greater than unity for non-cooperative systems in Quadrants III and IV. In other words, in order to achieve a TPF of 0.5, systems in Quadrants I/II require positive cooperativity while those in Quadrants III/IV require negative cooperativity.

Although the TPF value for any system can be determined using eq 7 (or eq S37), formulas describing width perturbations are somewhat more complex. Of course, such expressions are particularly important for systems with TPF values in excess of 0.5 ($\alpha > \alpha_{crit}$).[49] Therefore we have derived general expressions relating both TF_{50} and TI_{50} to known parameters, which enable one to determine the width perturbation for any system with a TPF greater than or equal to 0.5. Simplification of these expressions invoking the dominance assumption yields the Quadrant-specific relationships shown in Figure 4. Comparison of these expressions with their non-cooperative counterparts (Figure 2B) reveals several interesting features. In general, TF_{50} values all scale inversely with respect to α, approaching a value one-half that of the limiting terminal species, while TI_{50} values all increase linearly with respect to α ad infinitum.

Cooperative Experimental Systems. As demonstrated above, the effects of cooperativity can alter potency (TF_{50}), efficacy ($[ABC]_{max}$), and dynamic range (TF_{50}–TI_{50}), depending on the system. Our model provides the first general description of how to gain both qualitative and quantitative understanding of these effects. Application of our model to published experimental data enables direct calculation of α as well as an understanding of the specific effects of cooperativity on the dose–response curve critical points.

For example, access to eqs 7 (TPF) and S205 (Figure 4, Quadrant III) greatly facilitates the quantitative determination of α. This fact is demonstrated through investigations into a

class of ternary photocurrent-generating electron-transfer complexes built from a photoactive electron donor ("fluorophore"), a linker, and an electron acceptor ("quencher", Figure 5A).[4] Thus, based on the values reported for the terminal species concentrations and binary dissociation constants, the behavior of this system under non-cooperative conditions can be estimated (black curve). Because the observed dose–response curve (Figure 5A, orange curve) is narrower and smaller than that predicted under non-cooperative conditions, one can assume this system exhibits negative cooperativity. Indeed, by rearranging eq 7, we can directly estimate α at 0.09 from the observed value of $[ABC]_{max}$. This value is almost identical to that reported in this study (0.11),[50] which was determined through extensive experimental manipulations.[4] Furthermore, eqs 7 and S205 accurately predict the height ($[ABC]_{max}$) and width (TF_{50} and TI_{50}) of the curve, respectively, using reported values for cooperativity.

The behavior of ternary complex equilibria formed from major histocompatibility complex (MHC) proteins, bacterial superantigens, and T-cell receptors (TcR) provides perhaps a more sophisticated test of our analytical model.[51,52] In this system, the superantigen component brings together complementary regions of MHC and TcR proteins, which interact with each other in a manner reflecting positive cooperativity. Experimental data (Figure 5B, black dots) derived from plotting surface plasmon resonance frequency as a function of superantigen concentration reveals a large width perturbation compared to the predicted non-cooperative curve (black curve).[20] Because the y-axis values are not normalized for this data set, unlike for the previous example, we cannot use $[ABC]_{max}$ to calculate the magnitude of positive cooperativity directly. Instead, the magnitude of the cooperative width perturbation proves useful to this end. By rearranging the Quadrant III $\alpha > \alpha_{crit}$ TF_{50} and TI_{50} equations in Figure 4 (eqs S191 and S192), we can estimate α to be 10, which is similar to the value ($\alpha = 16$) determined in this study using more complex methods.[20]

Although we have described a comprehensive conceptual framework for ternary complex equilibria, one must exercise some caution in implementing its conclusions. For example, dominance and resolvability assumptions cannot be applied in all systems. Although under most circumstances they only introduce low levels of error (SI, Sections 5D,E and 6E,F), the fully expanded analytical expressions can be utilized ($[B]_{t,max}$ eq S34; $[ABC]_{max}$, eq S37; TF_{50} and TI_{50}, − and + forms of eq S200), if preferred. Finally, we have provided resources in the use of our framework in the form of a flowchart for guiding the appropriate implementation of our models (Figure S21) and an Excel spreadsheet that automates graphical and numerical analyses based on available parameters (see SI). Taken together, the resources provided in this article have the potential to impact the ability of scientists to conceptualize and utilize reversible ternary complex binding in a range of scenarios.

ASSOCIATED CONTENT

Ⓢ Supporting Information

Derivations for all the results reported here, as well as Figures S1–S21, Tables S1–S6, eqs S1–S218, and an Excel file that incorporates our conceptual framework (critical point annotation) into simulations of ternary complex dose–response curves. This material is available free of charge via the Internet at http://pubs.acs.org.

AUTHOR INFORMATION

Corresponding Author

david.spiegel@yale.edu

Notes

The authors declare no competing financial interest.

ACKNOWLEDGMENTS

REFERENCES

(1) Langmuir, I. *J. Am. Chem. Soc.* **1916**, *38*, 2221.

(2) Streusand, V.; Björk, I.; Gettins, P.; Petitou, M.; Olson, S. *J. Biol. Chem.* **1995**, *270*, 9043.

(3) Macura, N.; Zhang, T.; Casadevall, A. *Infect. Immun.* **2007**, *75*, 1904.

(4) Otsuki, J.; Narita, T.; Tsutsumida, K.; Takatsuki, M.; Kaneko, M. *J. Phys. Chem. A* **2005**, *109*, 6128.

(5) Ollivier, J.; Shahrezaei, V.; Swain, P. S. *PLoS Comput. Biol.* **2010**, e1000975.

(6) Levchenko, A.; Bruck, J. *Proc. Natl. Acad. Sci. U.S.A* **2000**, *97*, 5818.

(7) This model deals exclusively with complexes of three unique components (A, B, and C), and assumes that A and C do not interact in the absence of the bridging species, B; thus, all references to ternary systems in this manuscript are to linear, A−B−C complexes and, unless stated otherwise, all binding curve presented represent the concentration of linear, A−B−C ternary complex concentration ($[ABC]$) as a function of $[B]_t$, with all other parameters held constant.

(8) Though we restrict our analysis to linear, A−B−C complexes, other multicomponent complexes can also elicit this behavior, including extended linear complexes (e.g., A−B−C−D), hub-like complexes (where B has multiple binding partners), cyclic species (where A and C can interact), and A−B−A systems, as discussed elsewhere.[25]

(9) Buxton, B. *J. Med. Res.* **1905**, *13*, 431.

(10) Rodbard, D.; Feldman, Y.; Jaffe, M.; Miles, L. *Immunochemistry* **1978**, *15*, 77.

(11) Hussey, S.; Muddana, S.; Peterson, B. *J. Am. Chem. Soc.* **2003**, *125*, 3692.

(12) Rezaie, A. *J. Biol. Chem.* **1998**, *273*, 16824.

(13) Mulgrew, K.; Kinneer, K.; Yao, X.; Ward, B.; Damschroder, M.; Walsh, B.; Mao, S.; Gao, C.; Kiener, P.; Coats, S. *Mol. Cancer Ther.* **2006**, *5*, 3122.

(14) Assuming that concentrations are equal to the thermodynamic activities of each component, these K_d values are directly related to standard Gibbs free energy changes that occur upon binding, and represent the ratio between concentrations of free and bound species at equilibrium.

(15) Please see the SI for more details concerning this equilibrium.

(16) Mack, E.; Perez-Castillejos, R.; Suo, Z.; Whitesides, G. M. *Anal. Chem.* **2008**, *80*, 5550.

(17) A special situation—termed a "competitive binding" equilibrium—arises when A and C are incapable of binding B simultaneously due to strong negative cooperativity. Under such conditions, no ternary complex is formed. Analytical descriptions of such competitive equilibria have been reported previously.[18]

(18) Wang, Z. X. *FEBS Lett.* **1995**, *360*, 111.

(19) De Lean, A.; Stadel, J.; Lefkowitz, R. *J. Biol. Chem.* **1980**, *255*, 7108.

(20) Andersen, P.; Schuck, P.; Sundberg, E.; Geisler, C. *Biochemistry* **2002**, *41*, 5177.

(21) Perelson, A. *Math. Biosci.* **1980**, *49*, 87.

(22) Segel, I. *Enzyme kinetics*; John Wiley & Sons: New York, 1975.

(23) Wofsy, C.; Goldstein, B.; Dembo, M. *J. Immunol.* **1978**, *121*, 593.

(24) Braun, P.; Wandless, T. *Biochemistry* **2004**, *43*, 5406.

(25) Bray, D.; Lay, S. *Proc. Natl. Acad. Sci. U.S.A* **1997**, *94*, 13493.

(26) Héritier, M. *Nature* **2001**, *414*, 31.

(27) Bugaev, K. *Phys. Part. Nuc.* **2007**, *38*, 447.

(28) Ercolani, G. *J. Phys. Chem. B* **1998**, *102*, 5899.

(29) Ercolani, G.; Scheiaffino, L. *Angew. Chem., Int. Ed.* **2011**, *50*, 1762.

(30) Borkovec, M.; Hamacek, J.; Pigut, C. *Dalton Trans.* **2004**, 4096.

(31) Yang, J.; Hlavacek, W. S. *Math. Biosci.* **2011**, *232*, 164.

(32) Griffiths, J. R. *Biochem. Soc. Trans.* **1978**, *6*, 258.

(33) $[ABC]_{max}$ is normalized with respect to $[A]_t$ here, as it is often the limiting reagent in noncooperative systems.

(34) Straus, O. H.; Goldstein, A. *J. Gen. Physiol.* **1943**, *26*, 559.

(35) Because the dominance assumption is never perfect (i.e., neither K_d will ever be zero), this plateau is not actually flat, and the precise position of $[ABC]_{max}$ can be determined using eq S37.

(36) Chapman, S.; Asthagiri, A. *Mol. Syst. Biol.* **2009**, *5*, 313.

(37) Bruckheimer, E.; Fazenbaker, C.; Gallagher, S.; Mulgrew, K.; Fuhrmann, S.; al., e. *Neoplasia* **2009**, *11*, 509.

(38) Taborda, C.; Rivera, J.; Zaragoza, O.; Casadevall, A. *J. Immunol.* **2003**, *170*, 3621.

(39) Goodner, K.; Horsfall, F. L. *J. Exp. Med.* **1935**, *62*, 359.

(40) Clementi, N.; Mancini, N.; Solforosi, L.; Castelli, M.; Clementi, M.; Burioni, R. *Int. J. Mol. Sci.* **2012**, *13*, 8273.

(41) Hoogenboom, H. R. *Nat. Biotechnol.* **2005**, *23*, 1105.

(42) Tabrizi, M.; Funelas, C.; Suria, H. *AAPS J.* **2010**, *12*, 592.

(43) Murelli, R.; Zhang, A.; Michel, J.; Jorgensen, W.; Spiegel, D. *J. Am. Chem. Soc.* **2009**, *131*, 17090.

(44) Gong, M. C.; Chang, S. S.; Sadelain, M.; Bander, N. H.; Heston, W. D. W. *Cancer Metastasis Rev.* **1999**, *18*, 483.

(45) Under these conditions, the A-B and B-C parameter sums differ by 100-fold, the ratio of K_{AB} to $[A]_t$ is approximately 1.5×10^5, and the ratio of $[C]_t$ to K_{BC} is approximately 100.

(46) Dubrovska, A.; Kim, C.; Elliott, J.; Shen, W. J.; Kuo, T. H.; Koo, D. I.; Li, C.; Tuntland, T.; Chang, J.; Groessl, T.; Wu, X.; Gorney, V.; Ramirez-Montagut, T.; Spiegel, D. A.; Cho, C. Y.; Schultz, P. G. *ACS Chem. Biol.* **2011**, *6*, 1223.

(47) Smith, G.; Craft, T. *Biochem. Biophys. Res. Commun.* **1976**, *71*, 738.

(48) Machovich, R.; Aranyi, P. *Biochem. J.* **1978**, *173*, 869.

(49) When the TPF values fall below 0.5, TF_{50} and TI_{50} values lose their dependence on α and approach constant values described by eq S201.

(50) We obtain the exact value (0.11) when using eq S36, of which eq 7 is a simplified form that assumes $[X]_t \gg [L]_t$, an assumption that is not entirely valid in this example.

(51) Saline, M.; Rödström, K.; Fischer, G.; Orekhov, V.; Karlsson, B.; Lindkvist-Petersson, K. *Nature Commun.* **2010**, *1*, 119.

(52) Wang, L.; Zhao, Y.; Li, Z.; Guo, Y.; Jones, L.; Kranz, D.; Mourad, W.; Li, H. *Nat. Struct. Biol.* **2007**, *14*, 169.